Article

The Deformation and Instability Characteristics of Fractured Landslides during Typhoon-Triggered Rainstorms: Observations from an In Situ Field Experiment

Taili Zhang [1,2], Jianbo Wu [2,*] and Qiang Sun [1]

[1] Nanjing Center, China Geological Survey, Ministry of Natural Resources, Nanjing 210016, China
[2] Key Laboratory of Geohazard Prevention of Hilly Mountains, Ministry of Natural Resources of China, Fuzhou 350002, China
*   Correspondence: wjianbo@mail.cgs.gov.cn

Abstract: Fractures are the dominant conditions for rainfall infiltration into slopes, which can aggravate the instability of landslides. However, few studies have been conducted to analyze in detail the instability and deformation characteristics of creeping landslides with fractures. In view of this, this study investigated a landslide in Fu'ao Village, Wencheng County, Zhejiang Province in China to determine how fractures affect landslide deformation and instability during heavy rainfall through an in situ simulation experiment. In the experiment, three consecutive days of rainfall were set up based on Typhoon Megi in 2016, and two conditions were simulated, namely, rainfall + water filling fractures and rainfall + filled fractures (also referred to as the first and second conditions, respectively). The changes in the volumetric water content (VWC), pore water pressure (PWP), and deep displacement of the landslide at a depth of less than 5 m under the two conditions were observed using field monitoring instruments. The simulation results were as follows: (1) The volumetric water content of the shallow soil showed a more sensitive time-varying response to rainfall, while that of the soil at a depth of more than 200 cm showed a lagged response to rainfall, with a lag of about 10 h, which decreased significantly in the case of the unfilled fractures; (2) Under the first condition, the pore water pressure at different depths showed almost the same changing amplitude of 5 kPa or less. Under the second condition, the pore water pressure increased significantly with depth during the rainfall, with the changing amplitude reaching 30 kPa; (3) The displacement of the borehole equipped with the inclinometers near the front of the slope was higher than that at the borehole equipped with the inclinometers near the rear of the slope. The displacement under the first condition was up to 6 mm, which was significantly greater than that under the second condition. Therefore, fractures have significant effects on the instability of landslides induced by typhoon-triggered rainstorms, and one important measure to prevent and control this type of landslides is to fill fractures in the landslides in time.

Keywords: typhoon; fracture; landslide; volumetric water content; pore water pressure; displacement

1. Introduction

China is one of the countries in the world that experience the most frequent typhoons and suffer the most severe destruction from typhoons [1,2]. The rainstorms triggered by typhoons usually result in numerous secondary geological disasters, such as landslides and mudslides, which cause severe property loss and casualties in local areas [3,4]. Therefore, it is of great significance to study the instability characteristics and deformation failure process of landslides during typhoon-triggered rainstorms.

Typhoon-triggered rainstorms are characterized by a short duration and high intensity [5,6]. They mainly induce two types of landslides: sudden sliding and reactivated creeping [7]. The landslides of the former type are mostly small-scale, shallow landslides and tend to occur in clusters under heavy rainfall [8,9]. In contrast, reactivated creeping

landslides generally occur on early unstable slopes [10], whose surfaces suffer tensile damage under the influence of rainstorms. As a result, the stress inside the slopes is redistributed, forming a new stable state of the slopes [11,12]. Reactivated creeping landslides can cause large-scale disasters at a low frequency, especially after their fractures are filled. Presently, most studies of landslides induced by typhoon-triggered rainstorms primarily focus on shallow landslides, including their instability mechanism [4,13], field monitoring [14,15], landslide inventory mapping [16], rainfall warning [17,18], stability simulation and analysis [19,20], and temporal–spatial probability assessment [21,22]. However, few studies have been conducted on the deformation, instability, and failure processes of creeping landslides under typhoon-triggered rainstorms. Based on the detailed investigation of a catastrophic landslide in Taiwan caused by Typhoon Morakot, Tsou et al. concluded that the fundamental factors for the occurrence of the landslide included structures, weathering, and gravitational slope deformation [23]. By using a high-resolution digital elevation model (DEM), Chigira et al. (2013) analyzed the topographic features and geological structures prior to the destabilization of a large-scale, deep landslide in Japan caused by Typhoon Talas [11]. Using an experimental site for in situ landslide monitoring, Guo et al. studied the migration patterns of the rainfall infiltration-induced wetting front of slopes with different geological and topographical conditions [24]. However, the above studies do not involve fractured landslides, where fractures significantly affect the seepage condition of slopes during heavy rainfall and, thus, cannot be ignored.

Mathematical analysis, numerical simulation, and physical model tests are currently used to investigate the deformation and instability of landslides caused by typhoon-triggered rainstorms [14]. For example, Liu et al. proposed a water–air two-phase flow model to simulate the rainfall infiltration process on a soil slope, and conducted a field experiment to realistically test the model [25].Hsu et al. simulated and analyzed the instability of a typhoon-induced shallow landslide in Taiwan using a two-dimensional numerical model [26]. Chen et al., Kim et al., and Wang et al. explored the seepage and deformation failure patterns of rainstorm-induced landslides through physical model tests [27–29]. In addition, some researchers proposed different infiltration models for heavy rainfall to explain the slope failure mechanism due to typhoon-triggered rainstorms [30,31]. Compared with the above methods, in situ field simulation experiments have high pertinence and data reliability and differ slightly from the actual geological conditions of slopes. For example, Gvirtzman et al. performed field experiments on two large-scale landslides to track water flow through unsaturated stratified loess deposits [32]. Similarly, Tu et al. and Chen et al. conducted a series of artificial rainfall experiments on loess slopes to investigate the surface infiltration process in unsaturated soiland the response of loess landslides to rainfall [33,34]. Zhou et al. tested the effect of rainfall on the stability of accumulation slopes using an in situ monitoring test [35]. However, it could be found that most similar studies were conducted for loess or accumulation slopes, and few of them focused on typhoon rainstorm-triggered landslides. Based on the above analysis, this study conducted an in situ field experiment on a typical creeping landslide with fractures in Wencheng County, Wenzhou City. We analyzed the internal dynamic mechanism of the slope before and after its fractures were filled by simulating the different conditions of typhoon-triggered rainstorms. The purpose of this study was to provide scientific guidance and suggestions for the prevention and control of creeping landslides with fractures.

2. Overview of the Study Area and the Landslide

The study area is located in Wencheng County, Wenzhou City, Zhejiang Province. It lies in the southern mountainous area of Zhejiang Province, with geographical coordinates of 119°46′–120°15′ E and 27°34′–27°59′ N and a total area of 1292.2 km^2. The study area inclines from northwest to southeast and is dominated by mountains and hills. Wencheng County has a subtropical monsoon climate and four distinct seasons. This county has an average annual precipitation of about 1800 mm, with the rainfall concentrated in the summer. Owing to its location on the coast in East China, the study area is struck by

typhoons almost every summer. As a result, a series of heavy rainfall events lead to numerous geological disasters. For instance, in 2015–2016, Zhejiang Province was struck by three severe typhoons that caused the most unprecedented rainfall events in a century. As a result, thousands of geological disasters occurred in regions such as Fujian and Zhejiang Provinces, resulting in dozens of deaths and economic losses of hundreds of millions of yuan [36,37].

In this study, a landslide in Fu'ao Village was selected as the in situ experimental site. This landslide is located at the junction of the national highway G322 in Fu'ao Village, Huangtan Town, Wencheng County, with a length of about 30 m, a width of 25 m, elevations of 338 m at the rear and 322 m in the front, and a manually cut free surface with a length of about 5 m. The overall topography of the landslide is gentle in the upper part and steep in the lower part, presenting a significantly negative topography. The strata where the landslide is located are composed mainly of gravel-bearing tuffs of the Cretaceous Chaochuan Formation, in which gravels with a diameter of 3–30 mm and a content of 50% or more are found. The strata are covered by a layer of elluvium–proluvium with a thickness of about 3 m. The completely–highly weathered layers of the strata have a thickness of about 10 m. No groundwater flows out of the toe of the landslide, and the groundwater burial depth is greater than 5 m. The whole slope is nearly bare, and little vegetation (shrubs) can be observed only at the crown of the landslide, with a height of approximately 4–5 m. A significant fracture with a width of 10–30 cm occurs at the rear of the landslide, which was therefore selected as the rainfall experiment site in this study (Figure 1).
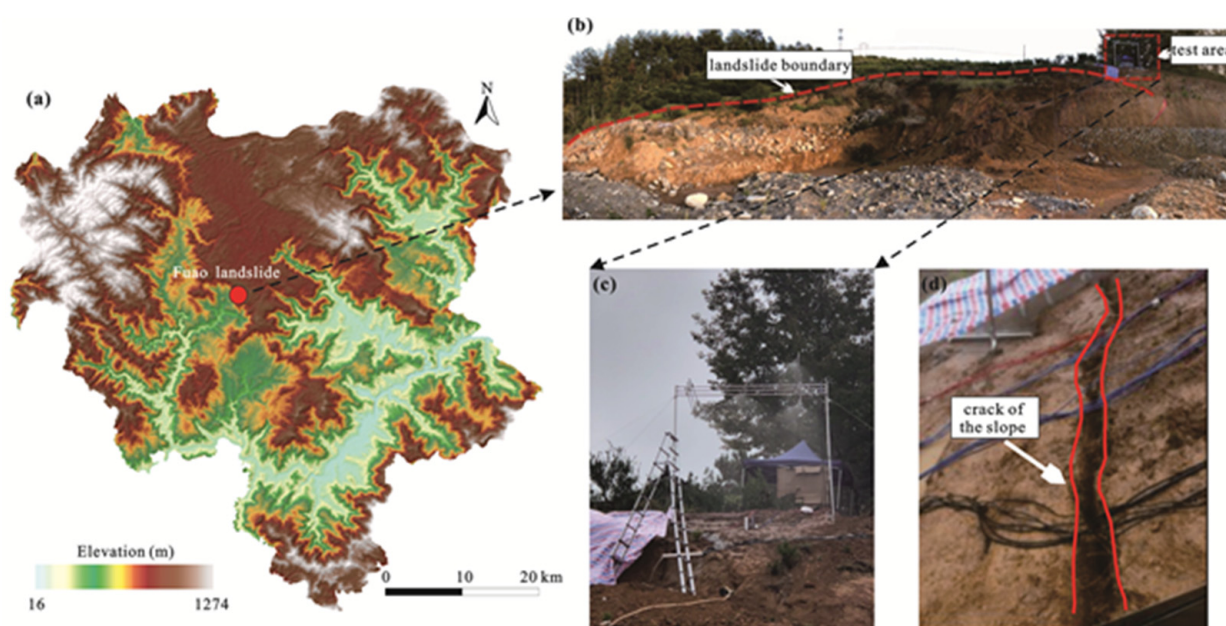
Figure 1. Location of the study area and the overall characteristics of the landslide in Fu'ao Village: (**a**) Digital elevation model (DEM) of Wencheng County, Wenzhou City; (**b**) Photo of the landslide in Fu'ao Village; (**c**) Photo of the experimental site; (**d**) Fracture at the rear of the landslide.

3. Setting and Process for the In Situ Landslide Field Experiment

3.1. General Layout of the Experimental Site

The experimental site for the landslide had a size of 4 × 4.5 m. It was surrounded by iron sheets with a burial depth of 80 cm on both sides as barriers (Figure 2a). A drainage ditch with a width of 20 cm and a depth of 10 cm was dug in the front and on the right side of the site. A catchment pool with a size of 2 × 2 × 1 m was dug in the front part of the site. The bottom and side walls of the drainage ditches and the catchment pool were plastered with cement. During the rainfall, all of the surface runoff was directed into the catchment pool through the drainage ditches (Figure 2b). Two boreholes were drilled in

the front and middle parts of the experimental site, and inclinometers were buried and fixed at different depths after the PVC pipes were placed into the boreholes. Another two boreholes were drilled on the left and right sides of the site to bury the pore pressure cells and soil hygrometers, respectively (Figure 2c).
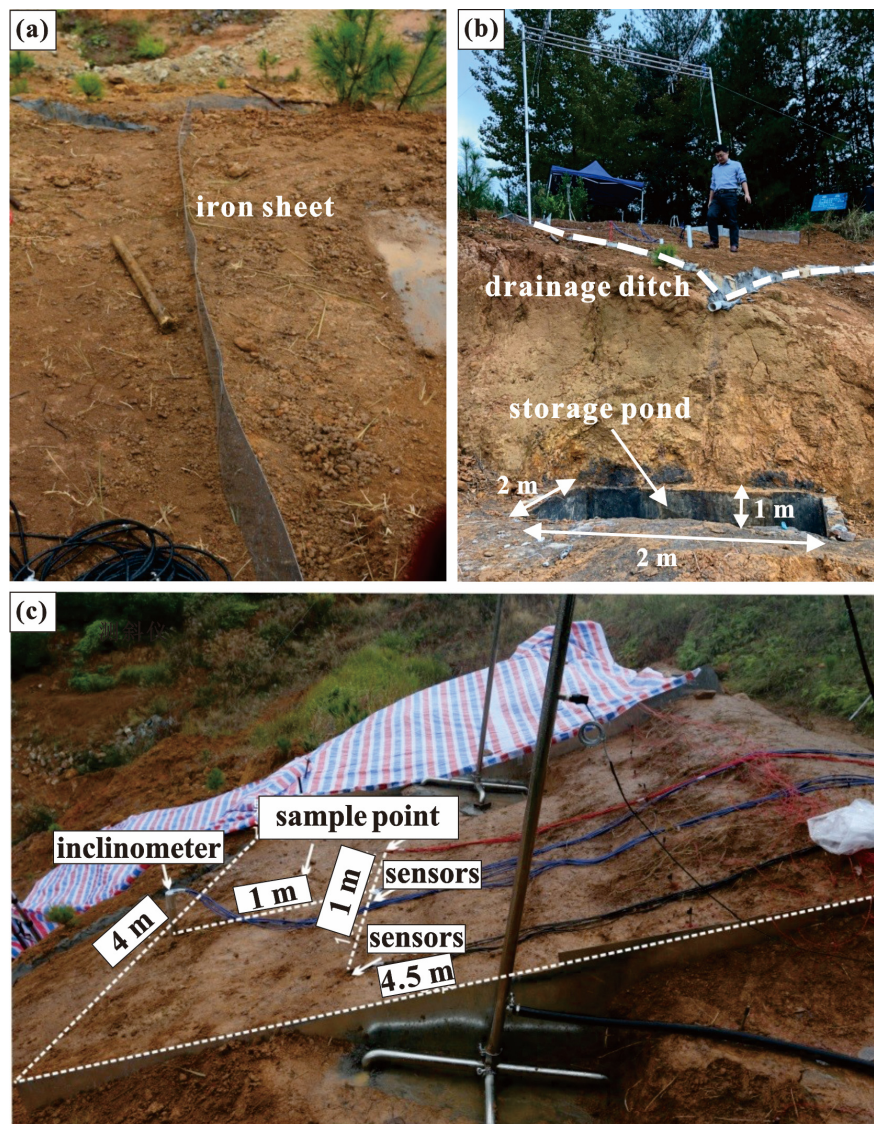
Figure 2. Layout of the experimental site of the landslide: (**a**) Iron sheets set on the site as boundaries; (**b**) Drainage and storage pool; (**c**) Rainfall area of the experimental site.

The installation of individual sensors was as follows: (i) The permeable pipe was installed into the borehole to place the sensors. (ii) The permeable stone at the bottom of the sensors was taken out and the sensors were placed into water for at least 24 h to exhaust the air. (iii) The water inlet of the sensors was wrapped with saturated gauze net in the water to make sure the sensors would not be blocked by silt during the measurement. (iv) The sensors were then placed into the pipe at different depths, and the soil was backfilled into the borehole. During this process, the cables connected with every single sensor were linked to the data collection system on the ground surface. (v) The sensitivity of the pipe and sensors were test by filling water into the borehole without rainfall. If the water table in the borehole decreased to the original condition or did not increase much, the sensitivity was considered as suitable. (vi) The mouth of the borehole was blocked with waterproof materials, and the installation was finished. In addition, the site was equipped with an artificial rainfall simulator, water, electricity, data collection instruments, and computers.

3.2. Field Monitoring Instruments and the Data Collection System

In this study, an automated data monitoring and collection system was used to primarily analyze three physical and mechanical indices, namely, volumetric water content, pore water pressure, and displacement. The purpose was to reveal the dynamic changes in the seepage and mechanical fields of the landslide during heavy rainfall. The specific information on the experimental instruments used in this study is shown in Table 1. An automated artificial rainfall simulation system (Figure 3a) was adopted for rainfall simulation and monitoring. The system was composed of a host controller, water tanks, water supply pipelines, water pumps, rainfall sprinklers, and metal supports. The host controller (Figure 3b) enabled artificial control over rainfall intensity and duration. To ensure sufficient water supply during the experiment, four domestic water tanks (Figure 3c) were installed on site, capable of storing 5.5 tons of water in total. Rotary down-spray sprinklers were employed in the experiment. They were small, medium, and large sprinklers, with nozzle diameters of 9 mm, 11 mm, and 13 mm, respectively.

Table 1. Instruments used in the experiment.

Instrument	Source	Type	Quantity	Measurement Index	Unit	Resolution	Accuracy
Portable automated artificial rainfall simulation system	Xinhuize Co., Ltd., Xi'an, China	XBJ-JY201	1	Rainfall	mm	0.01 mm	0.1 mm
Soil moisture sensor	Maihuang Co., Ltd., Hangzhou, China	MH-SFC	7	Volumetric water content	%	0.1%	±0.5%
Vibrating wire pressure cell for pore water	Dedu Co., Ltd., Changzhou, China	VP500	4	Pore water pressure	kPa	0.1 kPa	±0.01% of range
Micromachined-silicon in-place inclinometer	Jitai Co., Ltd., Nanjing, China	MI600	11	Deep displacement	mm	0.01 mm	±0.1% of range
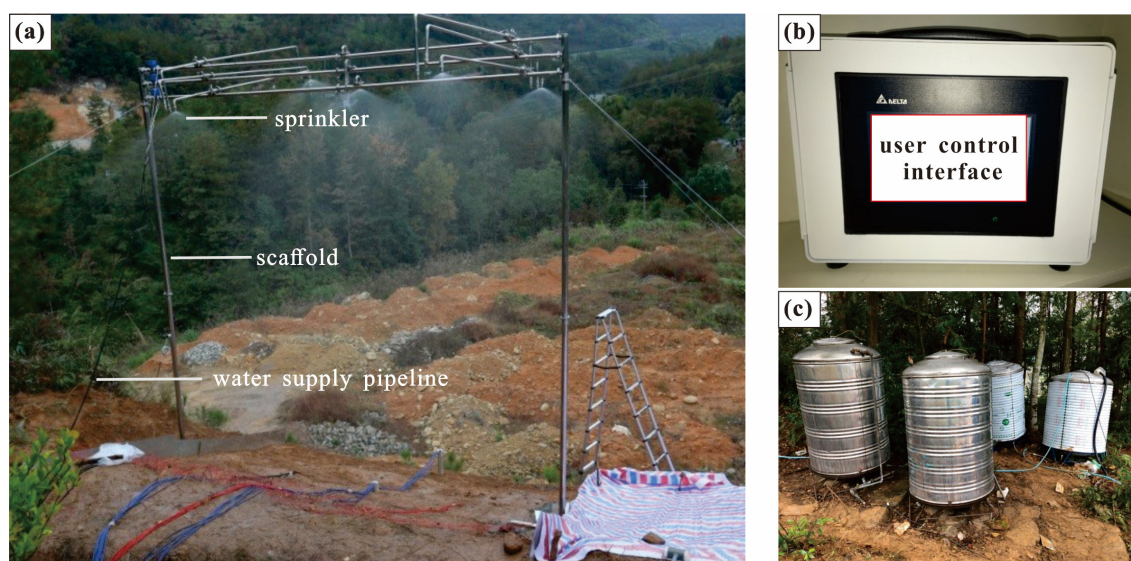
Figure 3. Automatic artificial rainfall simulation system: (**a**) General layout; (**b**) Control system; (**c**) Water tanks.

To reveal the patterns of changes in the physical indices inside the landslide affected by rainfall infiltration, the monitoring instruments were buried at different depths perpen-

dicular to the ground, with a maximum burial depth of 5 m. As shown in Figure 4a, an inclinometer casing was individually buried in the front and middle parts of the site. Six inclinometers were installed at burial depths of 40 cm, 100 cm, 200 cm, 300 cm, 400 cm, and 500 cm in the inclinometer casing buried in the front, while five inclinometers were installed at burial depths of 40 cm, 100 cm, 200 cm, 300 cm, and 400 cm in the inclinometer casing buried in the middle part. Four pressure cells for pore water and seven sensors for volumetric water content (VWC) were buried on the left and right sides of the site, respectively. The pore water pressure (PWP) cells had burial depths of 40 cm, 100 cm, 200 cm, and 300 cm, and the sensors for volumetric water content had burial depths of 10 cm, 30 cm, 50 cm, 75 cm, 125 cm, 200 cm, and 300 cm. Automatic data collection was adopted for each instrument, and the collected data were gathered in the instrument terminals (Figure 4b) for analysis.
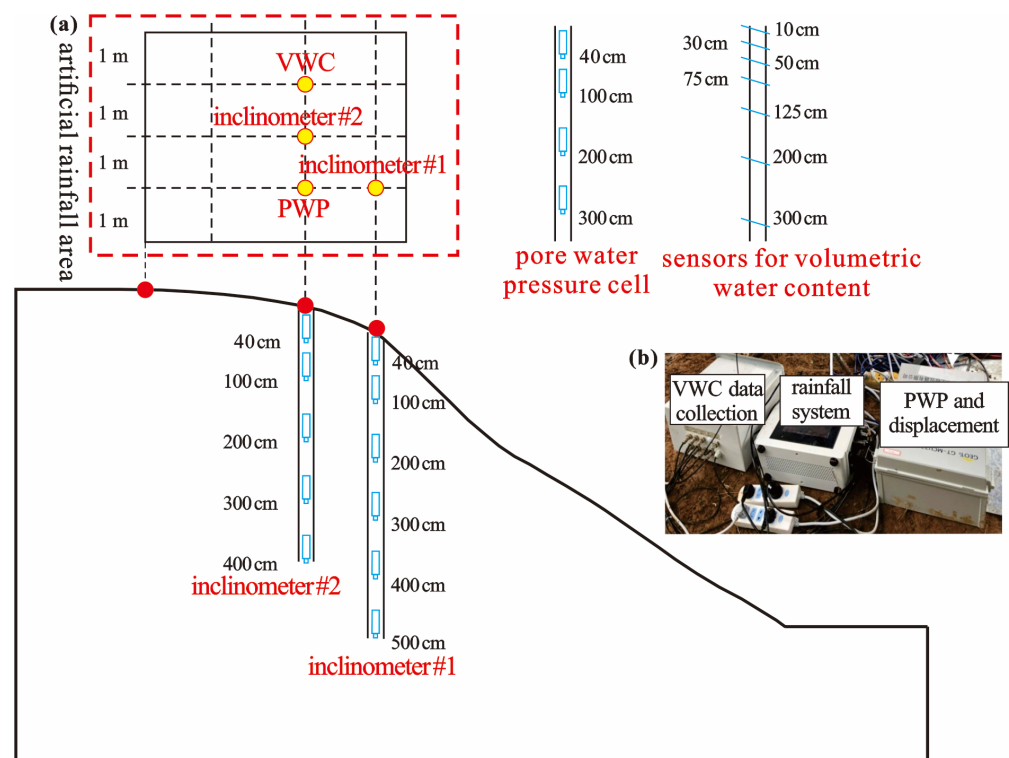
Figure 4. (**a**) Plan and profile setting of the sensors; (**b**) Controlling system of the sensors.

3.3. Rainfall Simulation Conditions

In recent years, the study area has been struck by many heavy rainfall events triggered by typhoons. The rainfall conditions were set up based on Typhoon Megi occurring during the rainy season in 2016. To investigate the influence of fractures on landslide deformation and instability, two rainfall conditions were set up in this study. The first condition was used to simulate the instability of the natural slope with filled fractures. The second condition was used to simulate the situation where fractures were filled with surface runoff (unfilled fractures) combined with typhoon-triggered rainfall. The rainfall model was set as follows (Figure 5): on the first day, the rainfall was 60 mm, with an intensity of 15 mm/h and a duration of 4 h; on the second day, the rainfall was 320 mm, with an intensity of up to 80 mm/h and a duration of 12 h; on the third day, the rainfall was 120 mm, with an intensity of 20 mm/h and a duration of 6 h. Therefore, the cumulative amount of precipitation was 500 mm. According to the measured value during the typhoon provided by the China Geological Survey, the landslide in Fu'ao Village had a rainfall amount of 497 mm (Figure 5), which was roughly consistent with the second condition set up in this study.
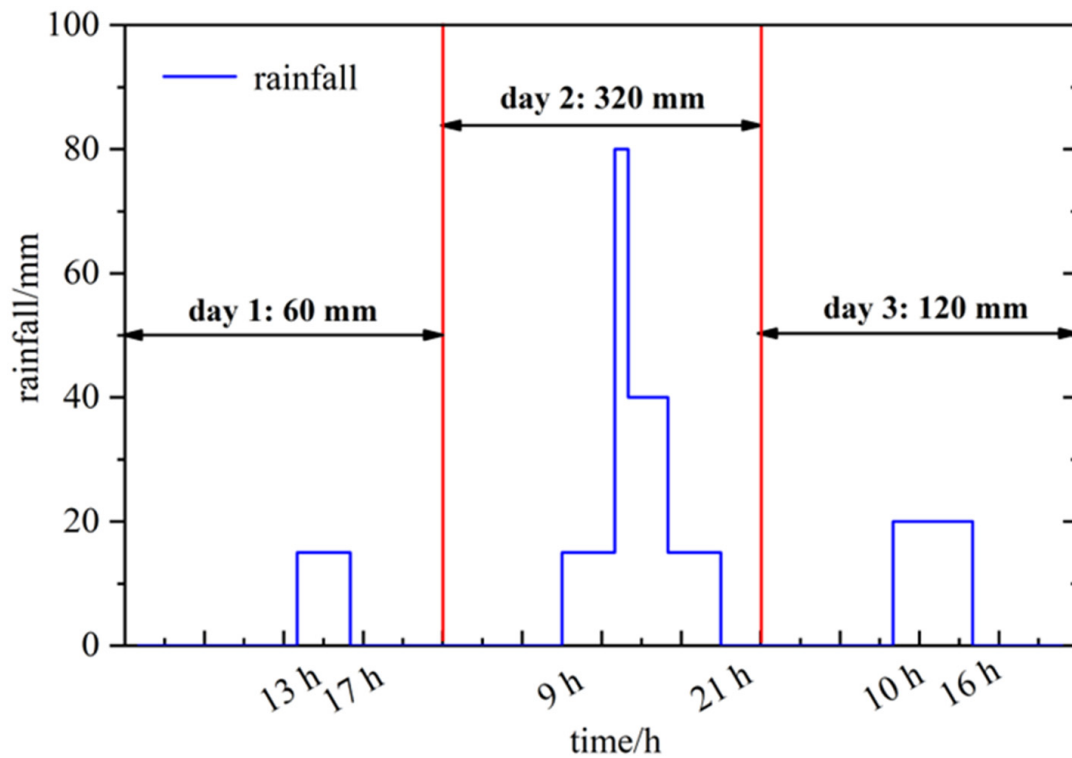
Figure 5. Rainfall simulation condition in this experiment.

4. Results

4.1. Time-Varying Response Characteristics of Volumetric Water Content

Figure 6 shows the changes in the volumetric water content at different depths under the first condition. The initial volumetric water content of the landslide at different depths was 41.2% (h = 10 cm), 23.4% (h = 30 cm), 37.8% (h = 50 cm), 22.3% (h = 75 cm), 24.5% (h = 125 cm), 17.5% (h = 200 cm), and 10.3% (h = 300 cm), as shown in the field experiment results:
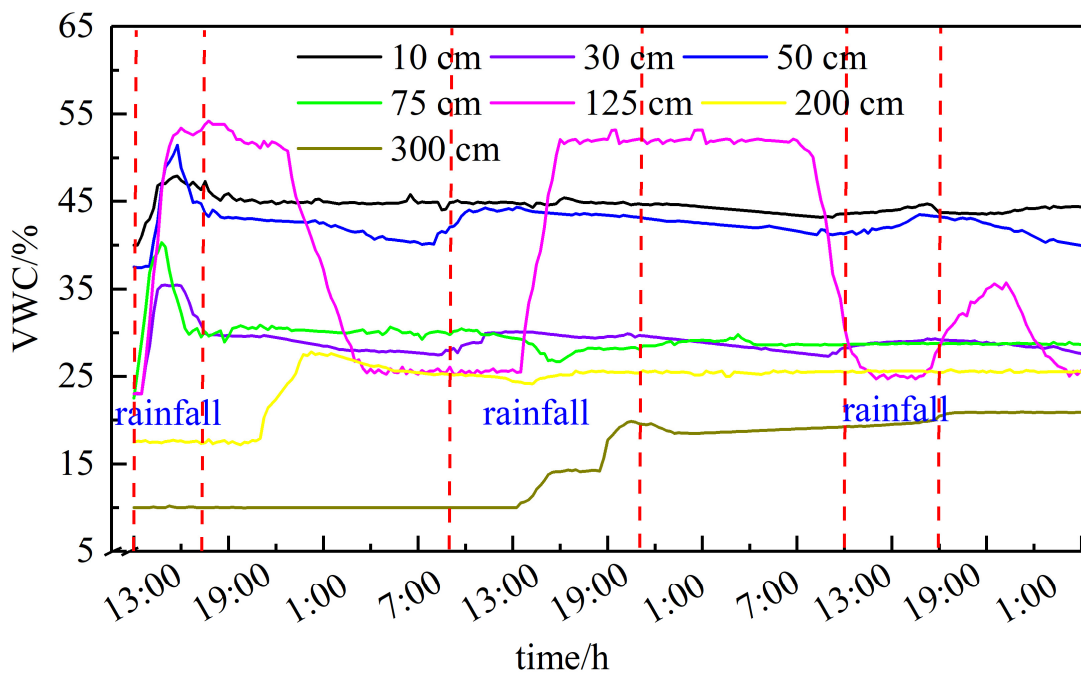
Figure 6. Time-varying curves of volumetric water content under the first condition.

The volumetric water content of the soil at a depth of 10–75 cm responded rapidly to the change in rainfall. It increased rapidly 0.5–1.5 h after the start of the rainfall, increasing from 41.2% to 49.8% at a depth of 10 cm, from 23.4% to 37.1% at a depth of 30 cm, from 37.8% to 50% at a depth of 50 cm, and from 22.3% to 40.6% at a depth of 75 cm. Subsequently, the volumetric water content of the soil decreased slightly while fluctuating and was finally stable at 33–35% or 43–45%.

Compared with that of the shallow soil, the volumetric water content of the soil at a depth of 125 cm was subject to more significant fluctuations. The volumetric water content at this depth increased rapidly from 24.5% to over 50% 2 h after the start of the first rainfall, and then decreased rapidly to about 27% 7 h after the first rainfall. It increased rapidly 5 h after the start of the second rainfall and began to decrease 1 h before the third rainfall. At the end of the third rainfall, it decreased to a minimum of 29.2%. The volumetric water content then increased again 2 h after the third rainfall, reached a maximum value of 35.3% 7 h after the third rainfall, and began to decrease slowly afterward. These results indicated that the volumetric water content of the soil at a depth of 125 cm exhibited a response lag to the rainfall infiltration, with the lag becoming increasingly long with the superposition of the rainfall events. This response lag was consistent with the results of a previous study [20]. The response lag of the volumetric water content to rainfall gradually increased with an increase in the soil depth. For the soil at a depth of 200 cm, its volumetric water content remained unchanged during the first rainfall and began to increase from 18.2% to 29.5% 10 h after the start of the experiment. For the soil at a depth of 300 cm, its volumetric water content did not vary significantly during the first rainfall and began to significantly increase 25 h after the start of the experiment (i.e., 7 h after the start of the second rainfall) with a small increase in amplitude from 10.6% to 20.8%, followed by low-amplitude changes.

Therefore, the landslide with the filled fractures (equivalent to the landslide without fractures) can be divided into three zones in the vertical direction according to the characteristics of the time-varying response of the volumetric water content to rainfall. The first zone had a depth of less than 75 cm, and its volumetric water content responded rapidly to the rainfall infiltration and increased rapidly. The second zone had a depth of about 125 cm. Its volumetric water content showed a slightly lagged response to the rainfall while fluctuating significantly and decreasing significantly after the rainfall. The third zone had a depth of more than 200 cm. Its volumetric water content showed a lagged response to the rainfall, with a lag of 10 h and above, and did not decrease significantly after increasing.

Figure 7 shows the changes in the volumetric water content of the soil at different depths under the second condition. For the soil at a depth of 10–50 cm, its volumetric water content was generally stable during the experiment, without showing significant fluctuations. This result indicated that the water filling the fracture at the rear had a slight effect on the soil at this depth. For the soil at a depth of 75–200 cm, its volumetric water content increased rapidly 2–3 h after the start of the first rainfall and fracture waterflooding and decreased rapidly to the original level after the first rainfall. The volumetric water content 0.5–3 h after the start of the second rainfall and water filling the fracture with water exhibited a response similar to that 2–3 h after the start of the first rainfall and water filling the fracture, followed by slight fluctuations. For the soil at a depth of 300 cm, more than 50% of its volumetric water content was retained after the second rainfall. These results indicated that the second condition had the most significant effect on the volumetric water content of the soil at a depth of 300 cm.

From the comparison of the above two experimental conditions, it could be concluded that the fracture near the rear of the landslide provided dominant seepage conditions for heavy rainfall. Therefore, in the case of unfilled fractures, the volumetric water content of the shallow soil exhibited a slight response to the rainfall, while that of the deep soil showed a response with a much shorter lag. In particular, at the end of the experiment, the soil at a depth of 200–300 cm had the maximum volumetric water content. This result indicated that water filling the fracture had severe effects on the soil at a depth of more than 200 cm, which might lead to deep sliding in the landslide in Fu'ao Village.
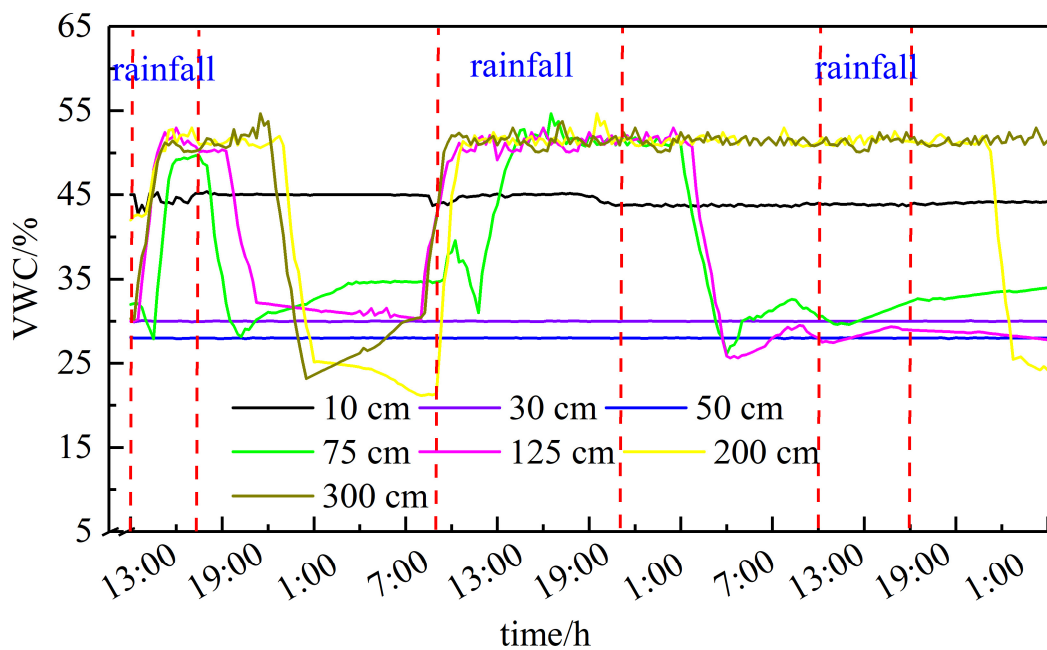
Figure 7. Time-varying curves of the volumetric water content under the second condition.

4.2. Time-Varying Response Characteristics of Pore Water Pressure

Figure 8 shows the changes in the pore water pressure monitored at depths of 40 cm, 200 cm, and 300 cm under the first condition. With an initial value of 0 kPa, the pore water pressure increased rapidly at different depths after the start of rainfall. The overall increased amplitude was inversely proportional to the depth. Specifically, the pore water pressure fluctuated within 5 kPa at a depth of 40 cm but fluctuated in a range of 0–3.5 kPa and 0–3 kPa, respectively, at depths of 200 cm and 300 cm. Moreover, the pore water pressure at different depths did not decrease significantly during the intervals between two adjacent rainfall events.

Figure 9 shows the changes in the pore water pressure monitored at depths of 100 cm, 200 cm, and 300 cm under the second condition, indicating significant differences from the first condition. First, the pore water pressure varied more significantly, reaching 12 kPa, nearly 20 kPa, and nearly 30 kPa for the soil at depths of 100 cm, 200 cm, and 300 cm, respectively. The responses were all quick, which was clear evidence for rapid infiltration into the soil. However, it should be noticed that this did not cause constantly wet soil conditions, because the pore water pressure dissipated more quickly and decreased rapidly during the intervals between two adjacent rainfall events. Especially for the sensor buried 100 cm below the ground surface, it reached 12 kPa during the first rainfall but a smaller PWP during the next two events (Figure 9a). This meant that the rapid drainage occurred at this depth after the first rainfall, and the second and third rainfall did not result in the same soil wetness conditions. This observed result was similar to that in Chen et al. [34]. Overall, compared with the first condition, the pore water pressure of the deep soil was more sensitive to rainfall under the second condition. Therefore, it could be concluded that the pore water pressure of the soil at a certain depth increased at a higher rate than that of the shallow soil for fractured landslides during rainstorms.
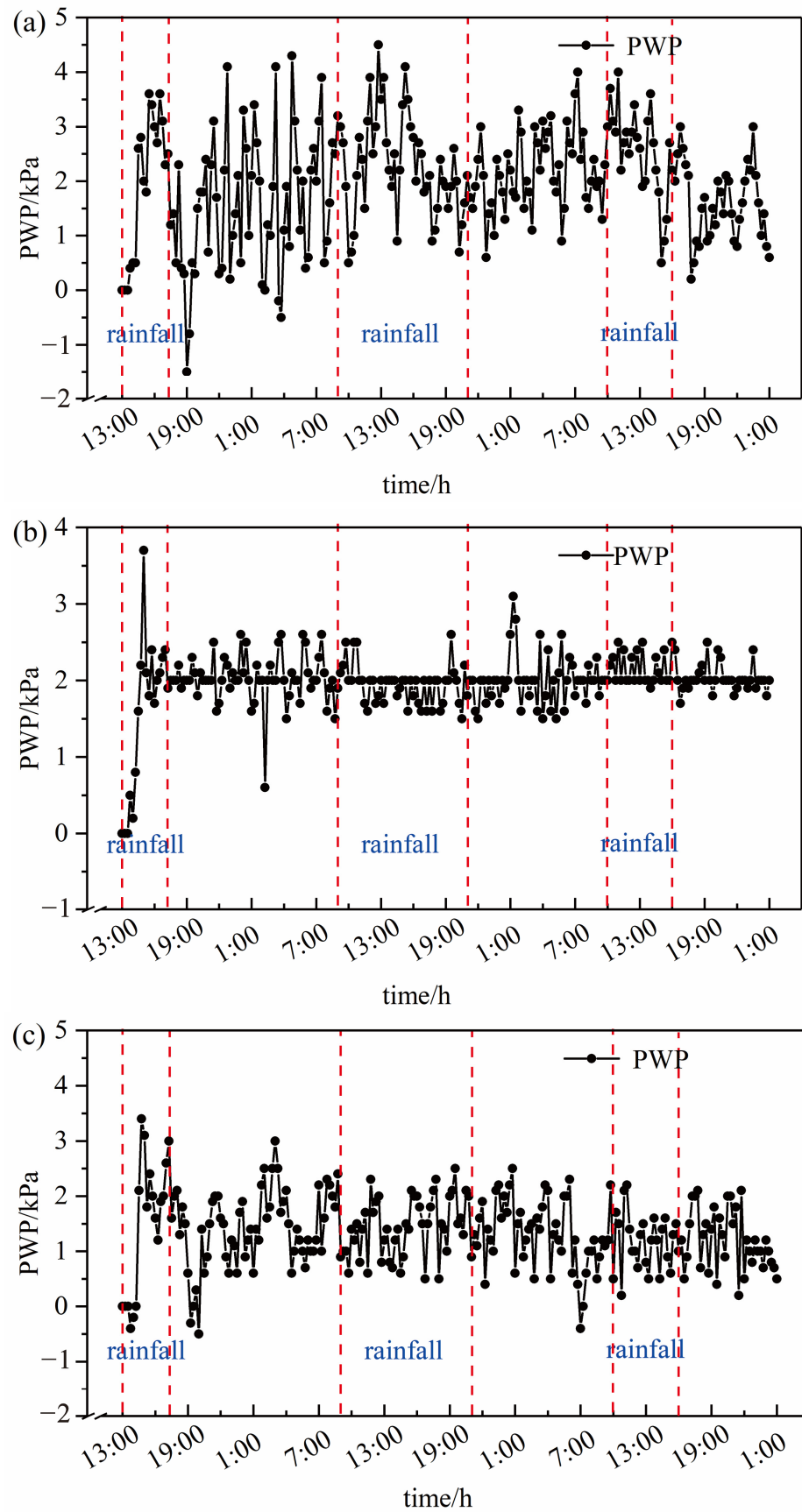
Figure 8. Time-varying curves of pore water pressure (PWP) at different depths under the first condition: (**a**) 40 cm, (**b**) 200 cm, and (**c**) 300 cm.
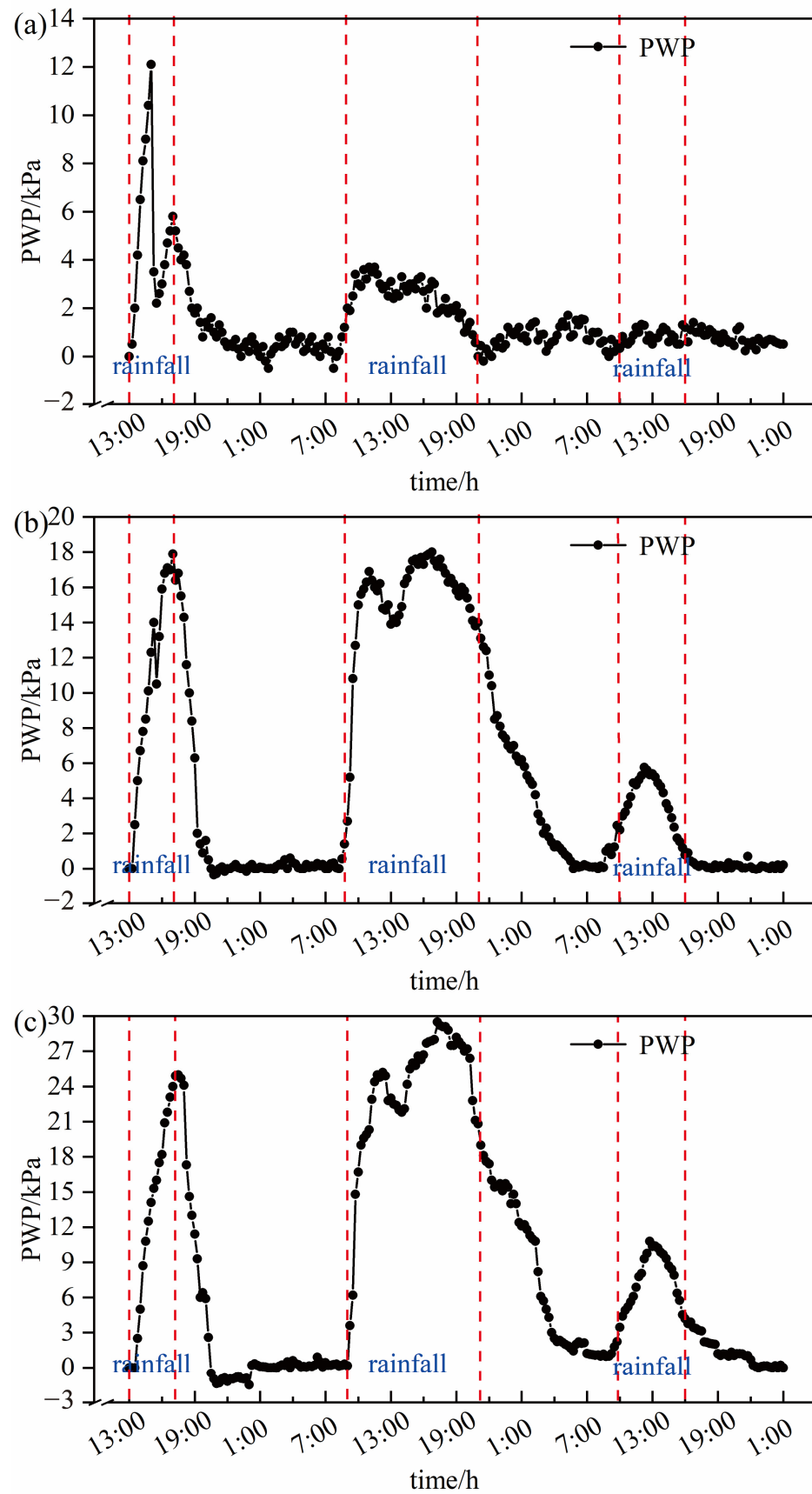
Figure 9. Time-varying curves of pore water pressure at different depths under the second condition: (**a**) 100 cm, (**b**) 200 cm, and (**c**) 300 cm.

4.3. Time-Varying Response Characteristics of Displacement

With the infiltration of rainfall, various parts of the landslide began to shift. Figure 10 shows the time-varying displacement curves of different positions in the two inclinometer casings under the first condition, indicating the following patterns of the changes in the displacement:

(1) The displacement at different depths increased significantly during each rainfall but stagnated or decreased after the rainfall. This result indicated that the displacement was sensitive to rainfall. In addition, the displacement was roughly inversely proportional to the depth, i.e., it gradually decreased from the shallow parts to the deep parts in the vertical direction. For instance, the maximum displacement at different depths in the No. 1 borehole equipped with inclinometers was 0.71 mm (40 cm), 0.55 mm (100 cm), 0.30 mm (200 cm), 0.17 mm (300 cm), 0.03 mm (400 cm), and 0.02 mm (500 cm) during the second rainfall. In addition, the positions at depths of 300–500 cm in both boreholes equipped with inclinometers had small cumulative displacement, indicating that the effective influence range of the first condition was roughly the zone with a depth of less than 300 cm.

(2) Compared to the No. 1 borehole equipped with inclinometers, both the No. 2 borehole equipped with inclinometers near the rear of the landslide and the position at the same depth in the No. 2 borehole equipped with inclinometers showed larger cumulative displacement. This indicated that the landslide in Fu'ao Village was more prone to failure in which displacement first occurred near the rear of the landslide and then gradually to the front of the landslide during typhoon-triggered rainstorms.

(3) According to the comparison of different rainfall periods, the No. 1 borehole equipped with inclinometers responded to different rainfall events, with the displacement increasing to different degrees; the No. 2 borehole equipped with inclinometers responded only to the former two rainfall events but showed small changes in the amplitude of the displacement during the last rainfall.

As shown in Figure 11, the time-varying curves of displacement in the inclinometer casings presented different characteristics under the second condition:

(1) The cumulative displacement increased significantly. The maximum cumulative displacement of the No. 1 borehole equipped with inclinometers at different depths was 3.03 mm (40 cm), 2.79 mm (100 cm), 2.56 mm (200 cm), 2.49 mm (300 cm), 1.78 mm (400 cm), and 2.56 mm (500 cm), and that of the No. 2 borehole equipped with inclinometers was 5.82 mm (40 cm), 2.15 mm (100 cm), 1.40 mm (200 cm), 1.20 mm (300 cm), and 0.25 mm (400 cm). They were all significantly larger than those of the first condition. Moreover, the second condition also presented a larger increased amplitude of cumulative displacement. These results indicated that the second condition was more likely to cause deep deformation of the landslide.

(2) For the positions at a depth of 400 cm and above, the cumulative displacement under the second condition was greater than that under the first condition. This result indicated that the presence of fractures would cause the affected parts within the landslide to shift downward in a wide range and possibly cause deep parts to slide. This occurred also because the fracture provided dominant seepage pathways. As a result, rainfall could reach the interior of the landslide more quickly than the surface infiltration of rainfall.

(3) It was interesting that the displacement values decreased after the rainfall ended in both conditions. The reason might come from two aspects: One is that the inclinometer in the borehole measured the deformation along the sliding direction of the slope. There was potentially a movement in another direction, reducing the displacement. In this condition, the slope was indeed moving but the direction was not the same as the initial one. Similar results were also observed in some other studies [34], which could lead us to conclude that even in the same profile or the same single point, the trend of displacement probably changes. Another reason is that the pore water pressure

might dissipate rapidly due to shear-induced dilation behavior, which subsequently led to the soil regaining strength [38]. Regardless of the reason, movement in the opposite direction of the predisposed landslide movement after the rainfall stops is questionable. Hence, it is important to mention and critically assess this phenomenon rather than avoiding it.
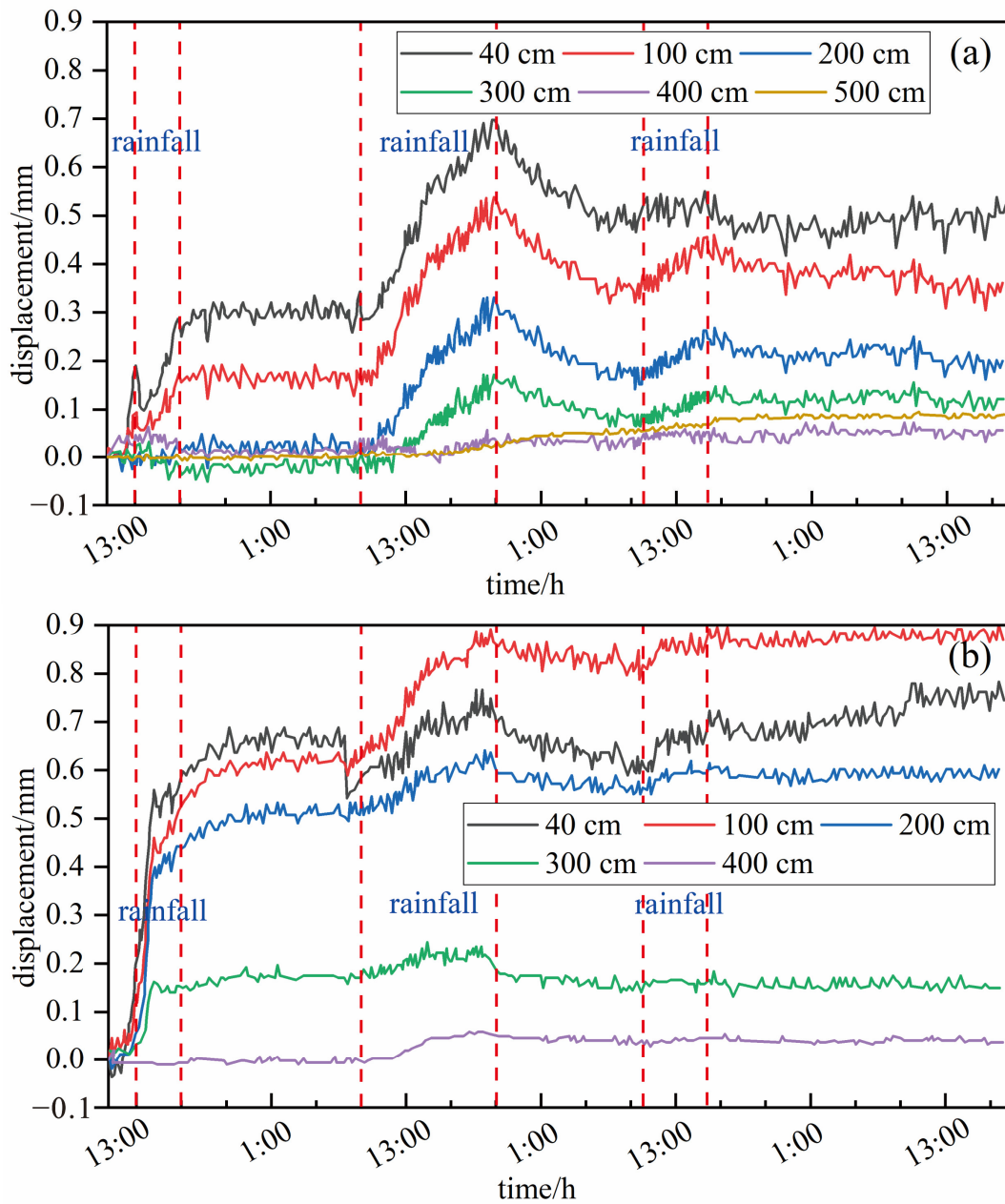
Figure 10. Displacement curves of different parts of the slope under the first condition: (**a**) No. 1 borehole equipped with inclinometers, (**b**) No. 2 borehole equipped with inclinometers.
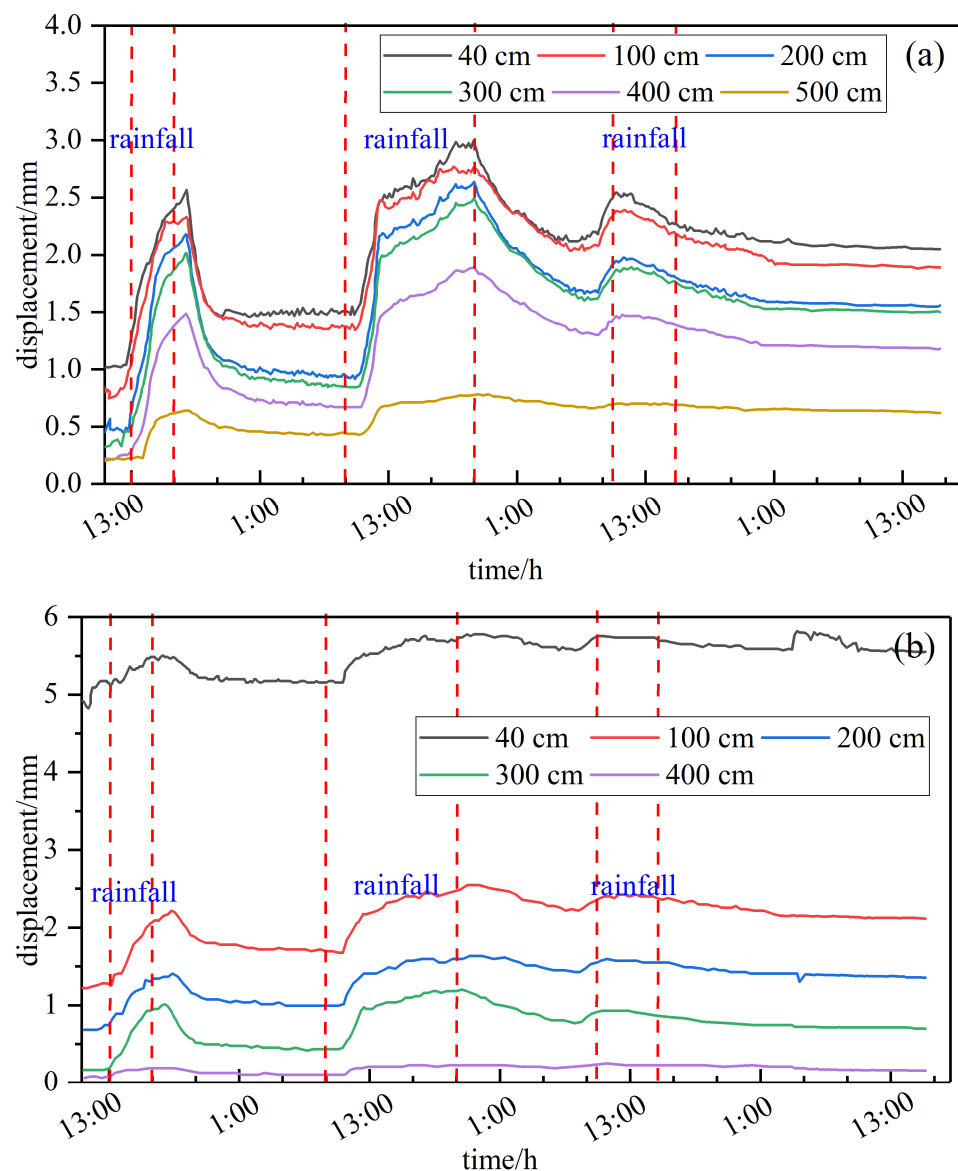
Figure 11. Displacement curves indifferent parts of the landslide under the second condition: (**a**) No. 1 borehole equipped with inclinometers, (**b**) No. 2 borehole equipped with inclinometers.

5. Discussion

Two major topics are discussed in this section. First, the spatial scale of the current study is compared with other studies, and second, the uncertainties that are associated with the results are clarified.

The present study focuses on a single landslide in a specific location (Zhejiang Province in China), so the outcomes from the test only make sense when they come to the slope scale. However, it should be noted that the in situ monitoring and test are still the closest way to model the realistic condition of the slope. This has been confirmed by some other studies, for example Tu et al. [33] and Chen et al. [34]. Some other methods to investigate rainfall infiltration in the soil layer exist, including physical model test. However, this kind of study is commonly based on the similarity principle, which means a specific slope with a certain of geometry is still necessary. For example, Prodan et al. utilized a physical model to evaluate the failure process in a landslide triggered by artificial rainfall, and a model platform with a length of 2.3 m, a width of 1.0, and a depth of 0.5 m was designed [39]. Wang et al. designed a physical model by taking the Dahua landslide in Yunnan Province of China as an example, to study the deformation and failure mechanism of deposit landslides

under a rainfall gradient [29]. Compared to these studies, we believe that the in situ test can provide some general insights that are related to all slopes. However, the rainfall scenario and geological conditions in this study are specific, only associated with a single typhoon event, and thus we have to admit that this aspect may limit the generalizability of the findings to other sites or other types of landslides.

The uncertainties regarding the potential sources of error or bias in the data are mainly related to one of the following aspects: (i) the limited duration of the experiment; (ii) the lack of consideration for the effect of vegetation on the slope stability; and (iii) the spatial heterogeneity of soil layer. Regarding the first aspect, three rainfall events were set during a three-day period, which fit with the accumulated rainfall triggered by a real historical typhoon event in the study area. In fact, the rainfall data record shows that typhoon events in the area normally last two to three days [22,24]; thus, the outcomes from the current observations mainly revealed the infiltration characteristics related to heavy rainfall. However, the antecedent recharge from general rainfall conditions has also been proven relevant to slope failure [40], which was not taken into account in this study. The second aspect is associated with the important role of tree roots in stabilizing slopes and consolidating the soil, which is mainly because roots can contribute to the total cohesion of the soil layer. In fact, some techniques have been proposed to quantify the effect of vegetation cover on slope stability, including the artificial root model in the laboratory [41], physically based model [42], and field monitoring [43]. However, there is no agreement on the specific effect of vegetation in the science community, which can be an essential factor to consider in our future work. It should also be noted that the results of hydrologic-mechanical time-varying characteristics are affected by the location of the sensors. Therefore, it would be better to set more monitoring profiles to include the spatial heterogeneity of the soil parameters. However, this was not possible in this study due to the economic cost, which was another potential source of uncertainty.

6. Conclusions

Based on an in situ experiment, this study monitored and analyzed in detail the dynamic characteristics of the soil parameters of a landslide triggered by the typhoon rainstorm in Fu'ao Village, Zhejiang Province (SE China). When water filled the fracture (the first condition), the volumetric water content (VMC) of the soil responded rapidly to the rainfall at a depth of less than 125 cm, with an increased amplitude of at least 10% within 1 h after the rainfall. However, the VMC showed a lagged response to the rainfall at a depth of more than 200 cm, with a lag of 10–30 h. When the fracture was filled (the second condition),the VMC of the soil varied slightly at a depth of less than 75 cm, fluctuated significantly at a depth of more than 125 cm, and reached its maximum at a depth of 300 cm. The pore water pressure (PWP) was sensitive to rainfall. Under the first condition, the changing amplitude of the pore water pressure at different depths was almost the same and did not exceed 5 kPa. Under the second condition, the pore water pressure increased significantly with an increase in the depth during the rainfall, with the changing amplitude reaching a maximum of 30 kPa. Regarding the slope deformation, the internal displacement of the landslide decreased roughly with an increase in the depth during heavy rainfall. The displacement in the borehole equipped with inclinometers near the front of the landslide was higher than that in the borehole near the rear of the landslide. The displacement under the second condition was significantly higher than that under the first condition, and they had a maximum displacement of 6 mm and 1 mm, respectively.

Overall, the current findings revealed the significant effect of fractures on the stability of the landslide during heavy rainfall. On the one hand, the VWC and PWP of the deep soil became more sensitive to rainfall because the fracture on the slope provided a dominant seepage pathway for rainfall infiltration. On the other hand, the front and middle parts of the landslide with the fracture filled by water showed significantly increased displacement. Therefore, one important measure to prevent and control fractured landslides is to fill fractures in the landslides.

References

1. Segoni, S.; Piciullo, L.; Gariano, S.L. A review of the recent literature on rainfall thresholds for landslide occurrence. *Landslides* **2018**, *15*, 1483–1501. [CrossRef]
2. Guo, Z.; Ferrer, J.V.; Hürlimann, M.; Medina, V.; Puig-Polo, C.; Yin, K.; Huang, D. Shallow landslide susceptibility assessment under future climate andland cover changes: A case study from southwest China. *Geosci. Front.* **2023**, *14*, 101542. [CrossRef]
3. Cui, P.; Chen, S.Q.; Su, F.H.; Zhang, J.Q. Formation and mitigation countermeasure of geo-hazards caused by Moarc Typhoon in Taiwan. *J. Mt. Sci.* **2021**, *28*, 103–105.
4. Ren, R.; Yu, D.; Wang, L.; Wang, K.; Wang, H.; He, S. Typhoon triggered operation tunnel debris flow disaster in coastal areas of SE China. *Geomat. Nat. Hazards Risk* **2019**, *10*, 562–575. [CrossRef]
5. Clàudia, A.; Bennett, G.L.; Matthews, A.J.; Matera, M.A.M.; Tan, F.J. The role of geomorphology, rainfall and soil moisture in the occurrence of landslides triggered by 2018 Typhoon Mangkhut in the Philippines. *Nat. Hazards Earth Syst. Sci.* **2021**, *21*, 1531–1550.
6. Guo, Z.; Tian, B.; He, J.; Xu, C.; Zeng, T.; Zhu, Y. Hazard assessment for regional typhoon-triggered landslides by using physically-based model—A case study from southeastern China. *Georisk Assess. Manag. Risk Eng. Syst. Geohazards* **2023**. [CrossRef]
7. Miyabuchi, Y.; Maeno, F.; Nakada, S. The October 16, 2013 rainfall-induced landslides and associated lahars at IzuOshima Volcano. *J. Volcanol. Geotherm. Res.* **2015**, *302*, 242–256. [CrossRef]
8. Medina, V.; Hürlimann, M.; Guo, Z.; Lloret, A.; Vaunat, J. Fast physically-based model for rainfall-induced landslide susceptibility assessment at regional scale. *Catena* **2021**, *201*, 105213.
9. Guo, Z.; Torra, O.; Hürlimann, M.; Medina, V.; Puig-Polo, C. FSLAM: A QGIS plugin for fast regional susceptibility assessment of rainfall-induced landslides. *Environ. Model. Softw.* **2022**, *150*, 105354.
10. Guo, Z.; Chen, L.; Yin, K.; Shrestha, D.P.; Zhang, L. Quantitative risk assessment of slow-moving landslides from the viewpoint of decision-making: A case study of the Three Gorges Reservoir in China. *Eng. Geol.* **2020**, *273*, 105667. [CrossRef]
11. Chigira, M.; Tsou, C.Y.; Matsushi, Y.; Hiraishi, N.; Matsuzawa, M. Topographic precursors and geological structures of deep-seated catastrophic landslides caused by Typhoon Talas. *Geomorphology* **2013**, *201*, 479–493. [CrossRef]
12. Guo, Z.; Chen, L.; Gui, L.; Du, J.; Yin, K.; Do, H.M. Landslide displacement prediction based on variational mode decomposition and WA-GWO-BP model. *Landslides* **2020**, *17*, 567–583.
13. Alonso, E.E.; Gens, A.; Delahaye, C.H. Influence of rainfall on the deformation and stability of a slope in overconsolidated clays: A case study. *Hydrogeol. J.* **2003**, *11*, 174–192. [CrossRef]
14. Hürlimann, M.; Coviello, V.; Bel, C.; Guo, X.; Berti, M.; Graf, C.; Hübl, J.; Miyata, S.; Smith, J.B.; Yin, H.Y. Debris-flow monitoring and warning: Review and examples. *Earth-Sci. Rev.* **2019**, *199*, 102981. [CrossRef]
15. Chang, K.J.; Tseng, C.W.; Tseng, C.-M.; Liao, T.C.; Yang, C.J. Application of Unmanned Aerial Vehicle (UAV)-Acquired Topography for Quantifying Typhoon-Driven Landslide Volume and Its Potential Topographic Impact on Rivers in Mountainous Catchments. *Appl. Sci.* **2020**, *10*, 6102. [CrossRef]
16. Hölbling, D.; Abad, L.; Dabiri, Z.; Prasicek, G.; Tsai, T.T.; Argentin, A.L. Mapping and Analyzing the Evolution of the Butangbunasi Landslide Using Landsat Time Series with Respect to Heavy Rainfall Events during Typhoons. *Appl. Sci.* **2020**, *10*, 630. [CrossRef]
17. Arattano, M.; Marchi, L. Systems and sensors for debris-flow monitoring and warning. *Sensors* **2008**, *8*, 2436–2452. [CrossRef]
18. Tsai, T.T.; Tsai, Y.J.; Shieh, C.L.; Wang, J.H.C. Triggering Rainfall of Large-Scale Landslides in Taiwan: Statistical Analysis of Satellite Imagery for Early Warning Systems. *Water* **2022**, *14*, 3358. [CrossRef]
19. Ku, C.Y.; Liu, C.Y.; Su, Y.; Xiao, J.E.; Huang, C.C. Transient modeling of regional rainfall-triggered shallow landslides. *Environ. Earth Sci.* **2017**, *76*, 570. [CrossRef]
20. Lin, C.H.; Lin, M.L. Evolution of the large landslide induced by Typhoon Morakot: A case study in the Butangbunasi River, southern Taiwan using the discrete element method. *Eng. Geol.* **2015**, *197*, 172–187. [CrossRef]
21. Hürlimann, M.; Guo, Z.; Puig-Polo, C.; Medina, V. Impacts of future climate and land cover changes on landslide susceptibility: Regional scale modelling in the Val d' Aran region(Pyrenees, Spain). *Landslides* **2022**, *19*, 99–118. [CrossRef]

22. Cui, Y.; Jin, J.; Huang, Q.; Yuan, K.; Xu, C. A data-driven model for spatial shallow landslide probability of occurrence due to a typhoon in Ningguo City, Anhui Province, China. *Forests* **2022**, *13*, 732. [CrossRef]

23. Tsou, C.Y.; Feng, Z.Y.; Chigira, M. Catastrophic landslide induced by Typhoon Morakot, Shiaolin, Taiwan. *Geomorphology* **2011**, *127*, 166–178. [CrossRef]

24. Guo, Z.H.; Jian, W.B.; Liu, Q.L.; Nie, W. Rainfall infiltration analysis and infiltration model of slope based on in-situ tests. *Rock Soil Mech.* **2021**, *42*, 1635–1647.

25. Liu, G.; Zhu, X.; Guan, J.; Tong, F. Field experiment of rainfall infiltration on a soil slope and simulations based on a water-air two-phase flow model. *J. Mt. Sci.* **2021**, *18*, 2159–2167. [CrossRef]

26. Hsu, Y.; Yen, H.; Tseng, W.; Jan, C. Numerical simulation on a tremendous debris flow caused by Typhoon Morakot in the Jiaopu Stream, Taiwan. *J. Mt. Sci.* **2014**, *11*, 1–18. [CrossRef]

27. Chen, Y.; Irfan, M.; Uchimura, T.; Zhang, K. Feasibility of using elastic wave velocity monitoring for early warning of rainfall-induced slope failure. *Sensors* **2018**, *18*, 997. [CrossRef]

28. Kim, M.S.; Onda, Y.; Uchida, T.; Kim, J.K.; Song, Y.S. Effect of seepage on shallow landslides in consideration of changes in topography: Case study including an experimental sandy slope with artificial rainfall. *Catena* **2018**, *161*, 50–62. [CrossRef]

29. Wang, H.; Jiang, Z.; Xu, W.; Wang, R.; Xie, W. Physical model test on deformation and failure mechanism of deposit landslide under gradient rainfall. *Bull. Eng. Geol. Environ.* **2022**, *81*, 66. [CrossRef]

30. Wu, S.; Chui, T.F.M.; Chen, L. Modeling slope rainfall-infiltration-runoff process with shallow water table during complex rainfall patterns. *J. Hydrol.* **2021**, *599*, 126458. [CrossRef]

31. Cui, G.; Zhu, J. Infiltration model in sloping layered soils and guidelines for model parameter estimation. *Hydrol. Sci. J.* **2017**, *62*, 2222–2237. [CrossRef]

32. Gvirtzman, H.; Shalev, E.; Dahan, O.; Hatzor, Y.H. Large-scale infiltration experiments into unsaturated stratified loess sediments: Monitoring and modeling. *J. Hydrol.* **2008**, *349*, 214–229. [CrossRef]

33. Tu, X.B.; Kwong, A.K.L.; Dai, F.C.; Tham, L.G.; Min, H. Field monitoring of rainfall infiltration in a loess slope and analysis of failure mechanism of rainfall-induced landslides. *Eng. Geol.* **2009**, *105*, 134–150. [CrossRef]

34. Chen, G.; Meng, X.; Qiao, L.; Zhang, Y.; Wang, S. Response of a loess landslide to rainfall: Observations from a field artificial rainfall experiment in Bailong River Basin, China. *Landslides* **2018**, *15*, 895–911.

35. Zhou, Z.; Wang, H.; Fu, H.; Liu, B. Influences of rainfall infiltration on stability of accumulation slope by in-situ monitoring test. *J. Cent. South Univ. Technol.* **2009**, *16*, 297–302. [CrossRef]

36. Qin, H.; He, J.; Guo, J.; Cai, L. Developmental characteristics of rainfall-induced landslides from 1999 to 2016 in Wenzhou City of China. *Front. Earth Sci.* **2022**, *10*, 1005199. [CrossRef]

37. Zhang, T.L.; Zhou, A.G.; Sun, Q.; Wu, J.B.; Wang, H.S.; Liu, Z.H. Characteristics of the groundwater seepage and failure mechanisms of landslide induced by typhoon rainstorm. *Earth Sci.* **2017**, *42*, 2354–2362, (In Chinese with English Abstract).

38. Iverson, R.; Reid, M.; Iverson, N.; LaHusen, R.; Logan, M.; Mann, J.; Brien, D. Acute sensitivity of landslide rates to initial soil porosity. *Science* **2000**, *290*, 513–516. [CrossRef]

39. Prodan, M.V.; Peranić, J.; Pajalić, S.; Arbanas, Ž. Physical Modelling of Rainfall-Induced Sandy and Clay-Like Slope Failures. *Adv. Mater. Sci. Eng.* **2023**, *2023*, 3234542.

40. Kim, S.W.; Chun, K.W.; Kim, M.; Catani, F.; Choi, B.; Seo, J.I. Effect of antecedent rainfall conditions and their variations on shallow landslide-triggering rainfall thresholds in South Korea. *Landslides* **2021**, *18*, 569–582. [CrossRef]

41. Lan, H.; Wang, D.; He, S.; Fang, Y.; Chen, W.; Zhao, P.; Qi, Y. Experimental study on the effects of tree planting on slope stability. *Landslides* **2020**, *17*, 1021–1035. [CrossRef]

42. Zhang, J.; Qiu, H.; Tang, B.; Yang, D.; Liu, Y.; Liu, Z.; Ye, B.; Zhou, W.; Zhu, Y. Accelerating effect of vegetation on the instability of rainfall-induced shallow landslides. *Remote Sens.* **2022**, *14*, 5743. [CrossRef]

43. Gonzalez-Ollauri, A.; Mickovski, S.B. Hydrological effect of vegetation against rainfall-induced landslides. *J. Hydrol.* **2017**, *549*, 374–387. [CrossRef]